Electrochemistry of Cu(II)–peptide complexes containing histidine residues
II. Anomalous current fluctuation in the reduction process of Cu(II)–GGH*

Kô Takehara** and **Yasushi Ide**

Laboratory of Chemistry, College of General Education, Kyushu University, Ropponmatsu, Chuo-ku, Fukuoka 810 (Japan)

(Received January 31, 1991)

Abstract

The electrochemical behavior of a Cu(II)–GGH solution with a mercury electrode has been investigated. Cu(II)–GGH showed anomalous current–potential and current–time characteristics in the electrode processes at the mercury electrode, which are described as follows. (i) Periodical current fluctuations and subsequent sudden cessation of the fluctuation were observed in the potential step measurement. (ii) Periodical current fluctuations were observed in the drop-life of a dropping mercury electrode in the potential region where the polarographic maximum appeared. (iii) Cyclic voltammogram showed irregular current fluctuations and a reversed current peak in the cathodic and the anodic runs, respectively. (iv) The half-wave potential of Cu(II)–GGH was fairly negative in comparison with that of other Cu(II)–oligopeptide complexes.

All of these phenomena were proposed to relate to the adsorption and desorption behaviors of the reduction product of Cu(II)–GGH. The differential equation was presented to simulate the periodicity observed in the potential step measurement and it is found that a relatively simplified equation well simulated the periodical phenomena.

Introduction

In recent years, the study of periodical phenomena has been one of the most interesting subjects in various fields including chemistry. After the pioneer work of Belousov [1] and the later work of Zhabotinsky [2], various types of periodical phenomena concerning chemical reactions have been discovered and extensively studied [3, 4].

In the electrochemical systems, several different types of periodical phenomena have been reviewed by Wojtowicz [5]. Among them, the periodicity observed during the electrocatalytic reaction is one of the most attractive regions in this field [6]. The overshoot phenomena of polarographic current have been well known as 'polarographic maxima'. However, there have been few reports which refer to the correlation between periodical phenomena and polarographic maxima. Maeda *et al.* recently reported the correlation of these phenomena which had been observed in a liquid/liquid interface [7].

Electrochemical investigations of Cu(II)–oligopeptides have been carried out by several researchers and the appearance of one predominant cathodic peak which corresponds to the two-electron reduction of the Cu(II) complex to Cu(0) has been reported [8, 9]. The present authors also discussed the electrochemical behaviors of the copper complexes with GHL, GHG and GH in a previous report [10]. However, few reports concerning the current anomaly observed in the reduction process of Cu(II)–oligopeptide complexes appear to have been published.

The aim of the present work is to study the mechanism of the generation of periodical current fluctuation and the relation between the current fluctuation and polarographic maxima. A reaction model is proposed to simulate the periodicity and is discussed in relation to the adsorption–desorption behavior of the Cu(II) complex.

Experimental

Materials

GGH and GHG were purchased from Peptide Institute and Sigma Chemical, respectively. All other

*Abbreviations: GGH = glycyl-glycyl-L-histidine; GHG = glycyl-L-histidyl-glycine; GHL = glycyl-L-histidyl-L-lysine.

**Author to whom correspondence should be addressed.

0020-1693/91/$3.50

chemicals used were of analytical reagent grade. All peptides and inorganic chemicals were used without further purification.

Sample solutions of Cu(II)–peptide were prepared by dissolving an equimolar mixture of copper chloride, $CuCl_2$, and peptide into distilled water. A Britton-Robinson buffer was used for the pH adjustment.

Electrochemical measurement

The electrodes used were the dropping mercury electrode (DME), the Metrohm EA-290 hanging mercury electrode (HMDE) or the PAR model 303 static mercury electrode (SMDE) for the working electrode; platinum wire for the counter electrode; and the saturated calomel electrode (SCE) or Ag/AgCl electrode for the reference electrode. All potential values are reported versus the SCE reference electrode.

A Fuso model 312 polarograph and an NF Electronic model 1930 function synthesizer were used for electrochemical measurements. A Fuso model 332 phase-sensitive detector was attached to the polarograph for alternating-current (a.c.) measurement. Fast signals were recorded by a YEW model 3655 wave analyzer.

For observing streaming of the solution, small amounts of charcoal particles were suspended in the solution and monitored through an optical microscope.

In electrocapillary measurements, each drop interval of DME was recorded by a Fuso model 922 electronic timer and averaged over 10 drop-times for each potential.

The supporting electrolyte used was a 0.1 M (M = mol dm^{-3}) potassium chloride, KCl, unless otherwise stated. Dissolved oxygen was removed by bubbling the solution with pure nitrogen gas. All measurements were carried out at 25 ± 0.5 °C.

Results

Voltammetry and polarography

Figure 1 shows a representative cyclic voltammogram of Cu(II)–GGH in 0.1 M KCl solution. Several peaks (c1) with irregular height and the reversed current peak (a1) were observed in the cathodic and the anodic processes, respectively.

The polarogram of Cu(II)–GGH in 0.1 M KCl exhibits a typical polarographic maximum at the rising part of the reduction wave and at the same potential region a periodical current fluctuation was observed in a drop-life of DME as shown in Figs. 2 and 3.

The half-wave potentials of some Cu(II)–peptide complexes are shown in Table 1 and it should be

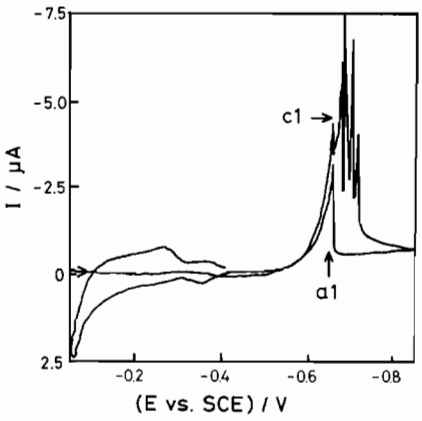

Fig. 1. Cyclic voltammogram of 0.5 mM Cu(II)–GGH solution at SMDE. Scan rate 50 mV/s, pH = 9.0.

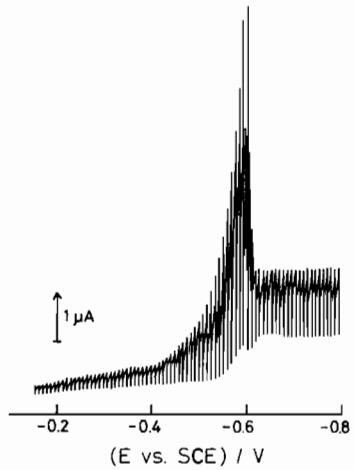

Fig. 2. d.c. polarogram of 0.5 mM Cu(II)–GGH solution at pH = 8.0. Scan rate 1 mV/s, drop time 4.0 s.

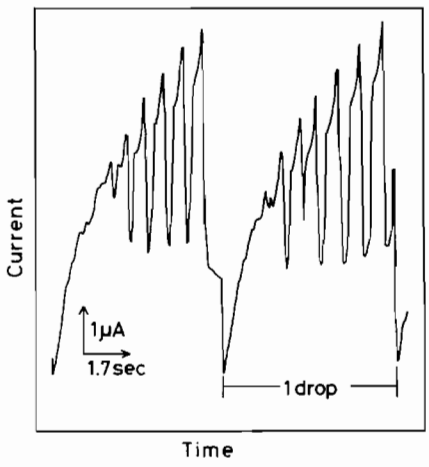

Fig. 3. Current–time curve of 0.5 mM Cu(II)–GGH solution in two drop-lives of DME. Electrode potential was −0.585 V (vs. SCE), pH = 8.0.

TABLE 1. Apparent half-wave potentials of some Cu(II)–peptide complexes at pH = 8.0

Peptides	$E_{1/2}$ vs. SCE (V)	
	Pre-wave[a]	Main-wave
Cu(II)–GH[b]	−0.22	−0.33(CV)[c]
Cu(II)–GHG	−0.12	−0.24
Cu(II)–GHL[b]	−0.15	−0.25
Cu(II)–GGH	−0.21	−0.51

[a]Refer to ref. 10 for the assignment of prewave and main-wave. [b]Cited in ref. 10. [c]Peak potential measured by cyclic voltammetry.

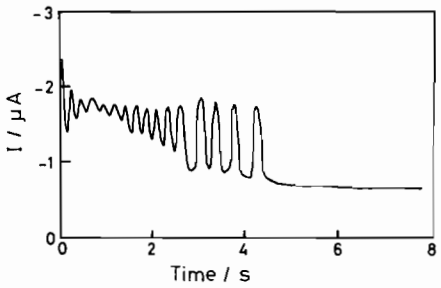

Fig. 4. Current–time curve of 0.5 mM Cu(II)–GGH at HMDE which recorded by potential step method. Initial potential −0.2 V, final step potential −0.63 V (vs. SCE), pH = 8.0.

noted that the value for the Cu(II)–GGH complex was fairly negative in comparison with those of other complexes.

Potential step measurement

In the potential step measurement, periodical current fluctuation and subsequent sudden cessation of the fluctuation was observed at the potential region where the polarographic maximum appeared (Fig. 4). The frequency of the fluctuation was nearly proportional to the final step potential. An increase of the Cu(II)–GGH concentration also increased the frequency, although a clear relationship between them could not be observed because of the appearance of random fluctuation at higher concentrations. On the other hand, a bi-frequency mode of periodical fluctuation was observed when the step potential was raised to −0.61 V as shown in Fig. 5.

By monitoring the charcoal particles suspended in the test solution, the acceleration of upward streaming tangential to the electrode surface was observed at the rising part of fluctuating current, while the streaming was slowed down to stop in the descending part of the current. Streaming of the solution was not observed at the potential region where no fluctuation occured.

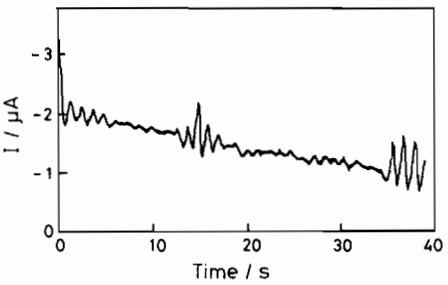

Fig. 5. Current–time curve of 0.5 mM Cu(II)–GGH at HMDE which recorded by potential step method. Initial potential −0.2 V, final step potential −0.61 V (vs. SCE), pH = 8.0.

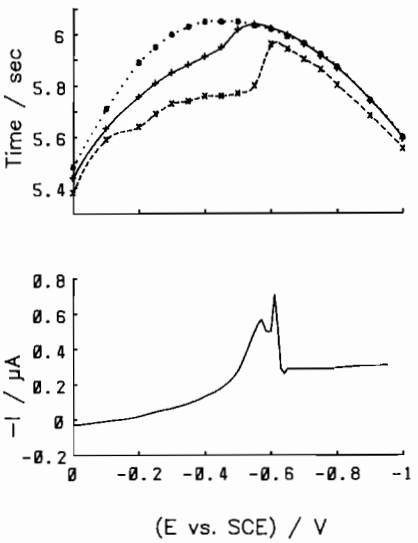

Fig. 6. Drop-time curve (upper) and a trace of polarogram (lower) for Cu(II)–GGH solution. In the drop-time curves, dotted, solid and broken line represents 0, 0.1 and 0.5 mM Cu(II)–GGH, respectively. All solutions contain 0.1 M KCl for supporting electrolyte and Britton-Robinson buffer to adjust the pH to 8.0. Concentration of Cu(II)–GGH in polarogram 0.1 mM.

Electrocapillarity

As shown in Fig. 6, the electrocapillary curve of the Cu(II)–GGH solution indicated the adsorption of the complex at a more positive potential than that of the polarographic maximum. The desorption potential was placed slightly negative to the electrocapillary maximum (ecm). The desorption potential of the Cu(II)–GGH solution was also more negative than those of other Cu(II)–peptides [10].

a.c. voltammetry

As shown in Figs. 7 and 8, the a.c. voltammogram of Cu(II)–GGH has a quite different profile from that of Cu(II)–GHG in which the current anomaly was not observed. In the capacitive current of Cu(II)–GGH (Fig. 7, Im), the potential where the

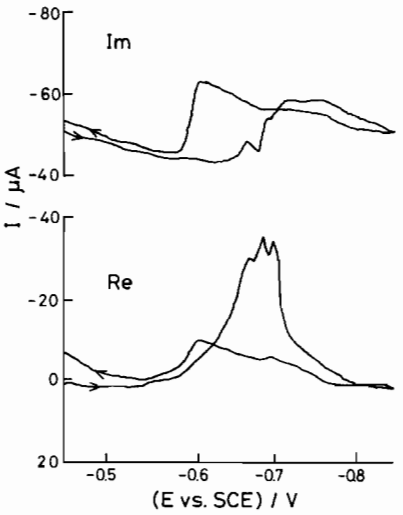

Fig. 7. Cyclic a.c. voltammogram of 0.5 mM Cu(II)–GGH at SMDE. Imposed a.c. frequency 100 Hz and amplitude 5 mV(rms), scan rate 50 mV/s, pH = 9.0. Upper trace (Im) and lower trace (Re) represent the imaginary and the real part of a.c. current, respectively.

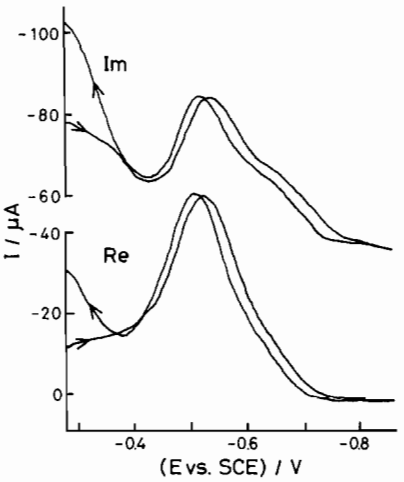

Fig. 8. Cyclic a.c. voltammogram of 0.5 mM Cu(II)–GHG at SMDE. Imposed a.c. frequency 100 Hz and amplitude 5 mV(rms), scan rate 50 mV/s, pH = 9.0.

current increased in the cathodic scan well coincided with that of the current fluctuation observed in potential step measurement. Furthermore, the potential where the current decreased abruptly in the anodic scan coincided with that of reversed current observed in the d.c. voltammogram (Fig. 1).

Discussion

Adsorption and desorption behaviors

The electrocapillary curve of Cu(II)–GGH indicates the adsorption of Cu(II)–GGH and/or its reduction product (Fig. 6). The blocking effect of adsorbed species to the following electrode reduction of Cu(II)–GGH is also indicated by the results mentioned as follows: (i) the reduction potential of Cu(II)–GGH coincided with the desorption potential of adsorbed species and (ii) the reduction of Cu(II)–GGH occurred at a more negative potential than other Cu(II)–peptide complexes. The following reduction of Cu(II)–GGH is restored only after desorption is completed. This issue is supported by the results of a.c. voltammetry, in which the abrupt increase of capacitive current was observed at the reduction potential of Cu(II)–GGH. The accumulation of Cu(0) on the mercury electrode was confirmed by the controlled-potential electrolysis of Cu(II)–GGH at a potential more negative than the desorption potential. The desorbing species then is attributed to the free GGH ion. The desorption potential of the adsorbed GGH was placed slightly negative to ecm and the adsorbed GGH is also considered to have a negative charge. The desorption, therefore, is caused by an electrostatic repulsion between the negatively charged electrode and the negatively charged GGH ion.

The abrupt decrease of the capacitive current observed in the anodic scan of the a.c. voltammogram indicates the re-adsorption of electrode species in the anodic process. Furthermore, the adsorbed species is ascribed to the reduction product of Cu(II)–GGH, Cu(0)–GGH, but not Cu(II)–GGH itself, because the reversed current (a1 in Fig. 1) was observed in the d.c. voltammogram at the same potential where the re-adsorption occurs.

As shown in Fig. 1, two re-oxidation peaks (*c.* −0 and −0.25 V) observed in the voltammogram indicate two different forms in the reduced species. The less negative peak obviously corresponds to the re-oxidation of copper amalgam, $Cu(0)_{amal}$, and the negative one can then be ascribed to the re-oxidation of Cu(0)–GGH.

From the above discussions, the following reactions were proposed for the electrode processes of Cu(II)–GGH: (i) most of the GGH ions remain at the mercury electrode after the reduction of Cu(II)–GGH; (ii) when the maximum adsorption was attained, the adsorbed GGH ions interfere in the following reduction of Cu(II)–GGH; (iii) the abrupt desorption of the GGH ion occurs at a slightly more negative potential than ecm, while Cu(0) remains at the mercury electrode as an amalgam.

Periodical current fluctuation

From the experimental results which show that the current fluctuation, the polarographic maximum, and the desorption of GGH occurred at the same

potential region, it is reasonable to consider that all of these phenomena are closely related to the adsorption and desorption processes.

Bauer [11] reviewed the origins of polarographic maxima as follows: (i) non-uniformity of the electric field at different positions of the electrode surface, (ii) non-radial growth of the mercury drop and (iii) non-uniform adsorption of the electrode species. In the present case, however, the second factor can be excluded because the current anomaly was observed even in the SMDE, the mercury growth of which is controlled by an electromagnetic valve. The third factor seems to be most likely for the origin of the maxima because of the participation of adsorption.

The following processes are considered for the generation of current fluctuation. The edge of the electrode capillary interferes with the flux of Cu(II)–GGH coming down to the upper part of the mercury drop, which causes the non-uniform adsorption of Cu(0)–GGH between the top and bottom of the mercury electrode. The gradient of surface tension caused by the non-uniform adsorption gives rise to the upward movement of the electrode surface and subsequently the streaming of the solution tangential to the electrode surface, which was confirmed by the movement of charcoal particles. The streaming of the solution brings about the increase of the reduction current at the bottom of the electrode, which is observed as a polarographic maximum. On the other hand, the inertia of mercury generates a time-lag in the motion of the electrode surface corresponding to the change of surface tension, which causes an excess adsorption of Cu(0)–GGH at the upper part of the electrode. When the surface coverage exceeds an upper limit, abrupt desorption takes place. These adsorption and desorption processes are repeated until the electrode characteristics are changed by the accumulation of $Cu(0)_{amal}$.

Simulation of periodical fluctuation

To confirm the reaction process mentioned above, the following set of equations is proposed for the simulation model:

$$\frac{dN_x}{dt} = I_x - \psi F_s - J_x \tag{1}$$

$$\frac{dN_y}{dt} = I_x + \psi F_s - J_y \tag{2}$$

$$\frac{dJ_y}{dt} = \alpha N_y - \beta J_y - \gamma \frac{dN_y}{dt} \tag{3}$$

$$\frac{dF_s}{dt} = \kappa(N_x - N_y) - \rho \frac{d(N_x - N_y)}{dt} \tag{4}$$

where the notations I, N, J and F_s denote the reduction current, the fractional surface coverage, the flux of desorbed species normal to the electrode surface and the flux of adsorbed species tangential to the electrode surface, respectively. The coefficients α, β, γ, κ, ρ and ψ were taken as parameters for the numerical simulation. The suffixes x and y mean bottom and top of the electrode surface, respectively. It is assumed that the difference of surface tension between the top and bottom of the electrode is proportional to the difference of surface coverage. Two assumptions $I_x \gg I_y$ and $J_x \ll J_y$, derived from the shield effect by the capillary edge, reduce eqns. (1) and (2) to more simple forms

$$\frac{dN_x}{dt} = I_x - \psi F_s \tag{5}$$

$$\frac{dN_y}{dt} = \psi F_s - J_y \tag{6}$$

With the assumption that the thickness of the diffusion layer, δ, is inversely proportional to the streaming of the solution, the faradaic current at the bottom can be expressed as

$$I_x = \frac{D}{\delta}(1 - N_x) = D(1 - N_x)(1 + F_s) \tag{7}$$

The symbol D contains the diffusion coefficient and the efficiency of the electrode reduction. The third term of eqn. (3) means the cooperative factor in the desorption process which takes place after the maximum adsorption. The second term in eqn. (4) means the time-lag factor of the movement of the electrode surface corresponding to the change of surface tension. The boundary conditions $N_x \geq 0$, $N_y \geq 0$ and $J_y \geq 0$ are derived from their physical meanings.

Figures 9–11 show the results of numerical calculations for some different conditions. The simulated

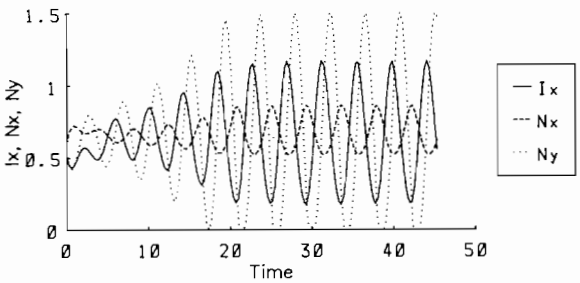

Fig. 9. Calculated curves of faradaic current (I_x) and surface coverage (N_x and N_y). Values of parameters; $D = 1.1$, $\alpha = 1.0$, $\beta = 1.0$, $\gamma = 0.8$, $\kappa = 1.0$, $\rho = 0.02$ and $\psi = 1.0$. In Figs. 9–11, solid, broken and dotted lines indicate I_x, N_x and N_y, respectively. Initial values of N_x and N_y are 0.6 and 0.4, respectively.

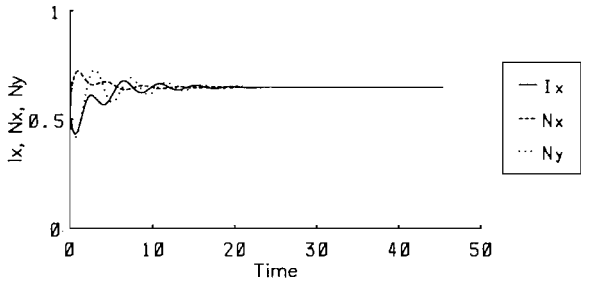

Fig. 10. Calculated curves of faradaic current (I_x) and surface coverage (N_x and N_y). Values of parameters; $D=1.1$, $\alpha=1.0$, $\beta=1.0$, $\gamma=0.2$, $\kappa=1.0$, $\rho=0.02$ and $\psi=1.0$.

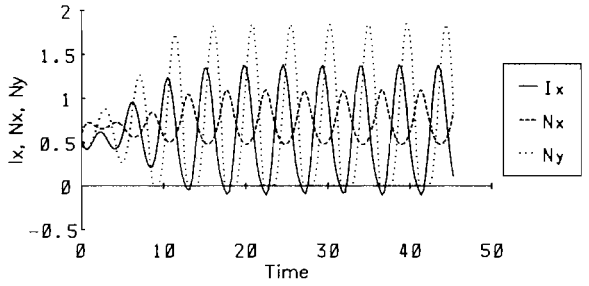

Fig. 11. Calculated curves of faradaic current (I_x) and surface coverage (N_x and N_y). Values of parameters; $D=1.1$, $\alpha=1.0$, $\beta=1.0$, $\gamma=0.8$, $\kappa=1.0$, $\rho=0.2$ and $\psi=1.0$.

current–time curves reproduce well the fundamental profile of the periodical current fluctuation. The results indicate that both the cooperative factor and the time-lag factor critically affect the generation and the profiles of periodical fluctuation (cf. Figs. 9 and 10). On the other hand, the frequency is sensitively affected by the rate of surface movement. Furthermore, the simulation showed that the surface coverage of the upper part, N_y, exceeds the full coverage ($N_y=1$) in some instances of fluctuation, which means excess adsorption beyond the monolayer coverage.

Under the conditions of a large time-lag of surface movement behind the change of surface tension (Fig. 11), the faradaic current, I_x, becomes negative after several periods of fluctuation, which indicates the limitation of eqn. (6) as an approximation of the faradaic current. Namely, this equation contains the implicit assumption that the adsorbed species completely blocks the following electrode process. In the real system, however, such a blocking effect is not so perfect and an excess adsorption will be attained in some instances even at the bottom of the electrode. The increase of the adsorption at the bottom of the electrode causes the decrease of the faradaic current, which results in the damping effect of the surface movement. Such a dumping effect will alter the fluctuation pattern after the excess adsorption. The calculated current–time curve will not then reproduce the real system in these regions.

The limitation of the equation mentioned above provides important information about the sudden cessation of periodical fluctuation observed in the real system (Fig. 4). The dumping effect caused by the excess adsorption reduces the differences in current density between the top and bottom of the mercury electrode. The accumulation of $Cu(0)_{amal}$, with progression of the electrode reaction, also alters the physical and chemical properties of the electrode surface. These two factors should be taken into account for the complete simulation of the sudden cessation of the faradaic current.

It is difficult to simulate the periodical fluctuation of current in the more complete form, because of the convection of the solution and of the non-linear factor of the time-lag effect. However, the periodical fluctuation of the faradaic current is simulated by the relatively simplified differential eqns. (1)–(7).

References

1 B. P. Belousov, in M. T. Grecova (ed.), *Autowave Processes in Systems with Diffusion*, USSR Academy of Sciences, Gorky, 1981, cited also in ref. 3 translated into English.
2 A. M. Zhabotinsky, *Biofizika, 9* (1964) 306.
3 R. J. Field and M. Bruger (eds.), *Oscillations and Traveling Waves in Chemical Systems*, Wiley, New York, 1985.
4 R. M. Noyes, *Ber. Bunsenges. Phys. Chem., 84* (1980) 295.
5 J. Wojtowicz, in J. O'M. Bockris and B. E. Conway (eds.), *Modern Aspect of Electrochemistry*, Vol. 8, Plenum, New York, 1970, p. 47, and refs. therein.
6 N. Fetner and J. L. Hudson, *J. Phys. Chem., 94* (1990) 6506, and refs. therein.
7 K. Maeda, S. Kihara, M. Suzuki and M. Matsui, *J. Electroanal. Chem., 295* (1990) 183.
8 M. Aihara, Y. Nakamura, Y. Nishida and K. Noda, *Inorg. Chim. Acta, 124* (1986) 169.
9 M. P. Youngblood and D. W. Margerum, *J. Coord. Chem., 11* (1981) 103.
10 K. Takehara and Y. Ide, *Inorg. Chim. Acta, 183* (1991) 195.
11 H. H. Bauer, in A. J. Bard (ed.), *Electroanalytical Chemistry*, Vol. 8, Marcel Dekker, New York 1975, p. 170.